Viscosity of mafic magmas at high pressures

C Cochain, Chrystèle Sanloup, C Leroy, Y Kono

AGU PUBLICATIONS

Geophysical Research Letters

RESEARCH LETTER
10.1002/2016GL071600

Key Points:
- Viscosity of pyroxene and olivine melts decreases with increased pressure up to 8 GPa
- Lower values of melt viscosity at higher pressures suggests tetrahedral ring units control viscosity
- A compilation of data obtained on melts shows that their viscosity converge toward a value of 20–30 mPa s at the highest *P* investigated

Correspondence to:
C. Sanloup,
chrystele.sanloup@upmc.fr

Citation:
Cochain, B., C. Sanloup, C. Leroy, and Y. Kono (2017), Viscosity of mafic magmas at high pressures, *Geophys. Res. Lett.*, *44*, doi:10.1002/2016GL071600.

Received 18 OCT 2016
Accepted 8 JAN 2017
Accepted article online 11 JAN 2017

Viscosity of mafic magmas at high pressures

B. Cochain[1,2], C. Sanloup[1], C. Leroy[3], and Y. Kono[4]

[1]Sorbonne Universités, UPMC Université Paris 06, CNRS, Institut des Sciences de la Terre de Paris, Paris, France, [2]Scottish Universities Physics Alliance (SUPA), School of Physics and Astronomy, University of Edinburgh, Edinburgh, UK, [3]Sorbonne Universités, UPMC Université Paris 06, CNRS, Institut de Minéralogie, de Physique des matériaux et de Cosmochimie, Paris, France, [4]HPCAT, Geophysical Laboratory, Carnegie Institution of Washington, Washington, District of Columbia, USA

Abstract While it is accepted that silica-rich melts behave anomalously with a decrease of their viscosity at increased pressures (*P*), the viscosity of silica-poor melts is much less constrained. However, modeling of mantle melts dynamics throughout Earth's history, including the magma ocean era, requires precise knowledge of the viscous properties of silica-poor magmas. We extend here our previous measurements on fayalite melt to natural end-members pyroxenite melts ($MgSiO_3$ and $CaSiO_3$) using in situ X-ray radiography up to 8 GPa. For all compositions, viscosity decreases with *P*, rapidly below 5 GPa and slowly above. The magnitude of the viscosity decrease is larger for pyroxene melts than for fayalite melt and larger for the Ca end-member within pyroxene melts. The anomalous viscosity decrease appears to be a universal behavior for magmas up to 13 GPa, while the *P* dependence of viscosity beyond this remains to be measured. These results imply that mantle melts are very pervasive at depth.

1. Introduction

The viscosity of depolymerized SiO_2-poor silicate melts at high *P* controls the dynamics of deep mantle melts in the present-day terrestrial planets, as their composition is controlled by olivine and pyroxenes. Because the viscosity of mantle melts determines their mobility, it also governs their ascent rates and consequently the degree of partial melting [*Stolper et al.*, 1981], as well as the extent of convection in magmatic bodies at depth. Komatiites in particular are the deepest mantle ultramafic melts, being generated at depths of 200 km or greater. The origin for the deepest komatiite melts lies at *P* greater than 9–10 GPa, possibly in a partially molten hydrated source from the top of the transition zone ~ 15 GPa [*Sobolev et al.*, 2016]. Their primitive composition suggests rapid transport toward the surface [*Nisbet*, 1982], which would be eased by very low viscosities at depth where the density contrast with the source rocks is expected to be very small [*Robin-Popieul et al.*, 2012].

The viscosity of depolymerized SiO_2-poor silicate melts at high *P* also controlled the dynamics of magma oceans within the first hundred million years following planetary formation [*Carlson et al.*, 2014]. Composition of the magma ocean could indeed be peridotitic as a high *P* cotectic liquid [*Zhang and Herzberg*, 1994]. Most models of magma ocean dynamics consider a viscosity range from 3×10^{-3} Pa s to 1 Pa s [*Solomatov*, 2000; *Hoink et al.*, 2006; *Maas and Hansen*, 2015]. These values are relevant for the dynamics of the early magma ocean with little crystallization, while later stages are controlled by the crystal fraction rather than by the viscosity of the liquid fraction. Coriolis forces are often considered negligible in the magma ocean dynamics [*Solomatov*, 2007]. However, Coriolis forces might have been important for a very low viscosity magma ocean in the early Earth due to faster rotation [*Maas and Hansen*, 2015], eventually leading to the flotation of crystals at intermediate mantle depths in equatorial zones. Similarly, metal droplets would have settled only at the poles during planetary differentiation but float above the equator for high-rotation rate and lower estimate for viscosity [*Moeller and Hansen*, 2013]. These studies, however, do not consider the *P*-induced variations of viscosity with depth, considering that the overall variation along a magma ocean adiabat would be within a factor of 10 as predicted from theoretical calculations [*Karki and Strixrude*, 2010]. In terms of depth (i.e., *P*), the extent of magma oceans is a debated topic, from magma ponds to planet-size magma oceans as planetesimals and terrestrial planets might have experienced either partial or full melting following accretion [*Elkins-Tanton*, 2012].

Theoretical estimations of magma viscosities differ from experimentally reported values, being lower by a factor of up to 10. Viscosity of molten diopside ($CaMgSi_2O_6$) was indeed experimentally found to be the lowest at the highest investigated *P*, i.e., 28 mPa s at 13 GPa and 2470 K [*Reid et al.*, 2003], while an increase from

Table 1. Mean Composition of the Quenched Samples (10 Analyses Per Composition)[a]

Oxide	$CaSiO_3$	$MgSiO_3$ #1	$MgSiO_3$ #2
SiO_2	50.94 (0.38)	59.3 (1.76)	58.8 (2.04)
MgO	0.09 (0.21)	34.71 (1.71)	36.14 (2.90)
Al_2O_3	0.63 (0.01)	0.28 (0.07)	2.38 (0.57)
CaO	46.62 (0.38)	1.18 (0.13)	1.02 (0.87)
FeO	0.08 (0.04)	2.80 (1.06)	0.62 (0.50)
H_2O	1.5 (0.2)	1.0 (0.1)	*
Total	99.24	99.27	98.97

[a]Data is given in oxide wt% along with the standard deviation in parenthesis. H_2O content was measured by ERDA; no $MgSiO_3$ #2 sample was analyzed by ERDA, but a similar H_2O content can be inferred from the totals.

20 mPa s at ambient *P* up to 60 mPa s at 13 GPa was theoretically predicted at 2500 K [*Verma and Karki*, 2012]. For molten $MgSiO_3$, molecular dynamics simulations along the 3000 K isotherm predict an initial decrease of the viscosity up to 5 GPa followed by a steep increase, while higher isotherms present a continuous viscosity rise [*Karki and Strixrude*, 2010]. Simulation boxes might be too small (less than 100 atoms) to capture a diffusing, rather large-scale process such as viscosity. Alternatively, experimental data using the falling-sphere method have been challenging to obtain in the past due to the low viscosities implied and the consequent low number of points collected during the fall of the sphere. Previous radiographic viscosity measurements on diopside melts under high *P* were done using lower time resolutions cameras available then (maximum 60 fps). Using high-speed camera, we reported a clear decrease of viscosity with increased *P* for molten fayalite Fe_2SiO_4 [*Spice et al.*, 2015] up to 9.2 GPa, an effect that could be related to the increase of Fe–O coordination number in the same pressure range [*Sanloup et al.*, 2013a].

We now need a comprehensive viscosity data set in the Ca-Mg-Fe-Si-O system. To avoid dealing with the complex situation of a sphere falling within a partially molten sample, the approach taken here is to work on end-member compositions rather than directly on a multicomponent composition with complex melting relationships. Three natural compositions of $CaSiO_3$ wollastonite and $MgSiO_3$ enstatite, two end-members of mantle pyroxenes, were chosen in order to obtain their viscosity versus *P* trend and their eventual variations with composition and provide a quantitative estimate of what can be expected at depth in the terrestrial mantle.

2. Materials and Methods

Samples consisted of grounded natural minerals, two different $MgSiO_3$ enstatite crystals (further referred to as $MgSiO_3$ #1 and $MgSiO_3$ #2), and $CaSiO_3$ wollastonite (cf. Table 1 for chemical analyses), obtained from the mineralogical collection at UPMC. Although no water was added to the initial powders, the quenched samples did contain between 1 and 1.5 wt% H_2O as measured by elastic recoil detection analysis (ERDA) at the nuclear microprobe of LEEL/NIMBE CEA (Laboratoire d'Etude des Elément Légers, Commissariat à l'Energie Atomique) Saclay [*Bureau et al.*, 2009], likely from diffusion from cell assembly materials. The effect of water on the viscosity of depolymerized melts has nonetheless been shown to be negligible at ambient *P* from $T = 1600$ K , i.e., at *T* far above the glass transition [*Whittington et al.*, 2000].

High *P-T* conditions were generated using a Paris-Edinburgh press at beamline 16-BM-B, High Pressure Collaborative Access Team (HPCAT) at the Advanced Photon Source, Argonne National Laboratory, USA. The cell assembly consisted of a graphite capsule surrounded by a MgO cylinder, following the design described in *Sakamaki et al.* [2012] and *Spice et al.* [2015]. *P* was measured from the cell volume of MgO as measured by in situ X-ray diffraction using the equation of state by *Kono et al.* [2010], and *T* was obtained from previous calibration [*Kono et al.*, 2014] tested against the melting curve of Fe within 20 K [*Kono et al.*, 2015] and against the melting curves of NaCl, KCl [*Kono et al.*, 2013], and fayalite [*Spice et al.*, 2015] within 50 K. For each sample, a rhenium sphere was loaded toward the top of the sample and covered by an additional thin sample layer in order to prevent contact with the graphite cap. At a given *P*, *T* was raised at 100 K/min either until melting for measurements along the melting curve or up to a submelting *T* point and then rapidly to the target *T* for measurements along an isotherm; power was shut after the sphere fell, which took between 0.4 s and 5 s, depending on the viscosity. The error bar on *T* is higher for points collected along an isotherm due

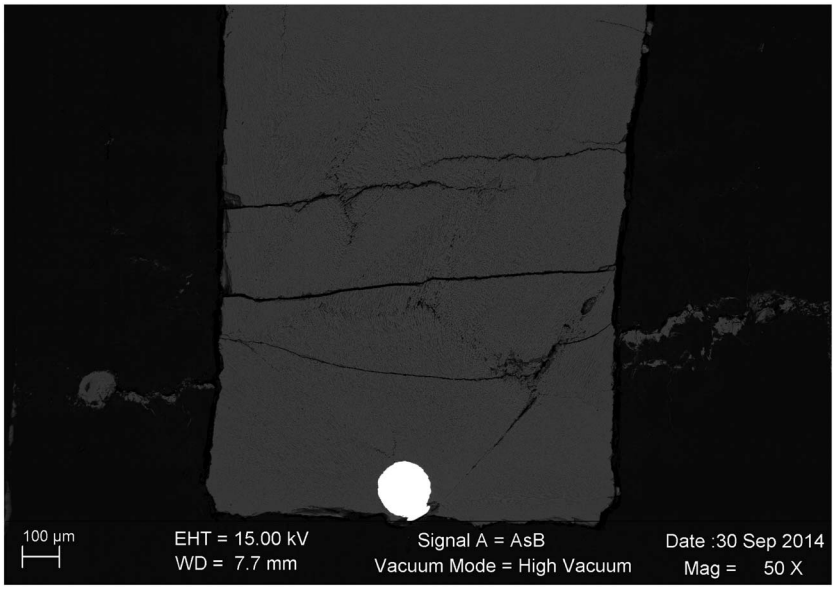

Figure 1. Scanning electron microscope image of a quenched sample ($MgSiO_3$ #1), with the Re sphere at the bottom of the graphite capsule.

to the unavoidable slight overshoot in the target power. After the experiments, samples were recovered and polished for further postmortem analyses. Scanning electron microscope analyses show that the Re sphere geometry was preserved (Figure 1) and did not react during the duration of the experimental run. Electron microprobe analyses were carried out at the CAMPARIS center at UPMC (Table 1) using a SX5 Cameca electron microprobe. Conditions were 15 keV and 10 nA.

3. Viscosity Data

Falling sphere viscometry measurements of molten silicates were made *in situ* at high *P-T* up to 7.6 GPa and 2243 K (Figure 2). Measurements were done along the melting curves for $CaSiO_3$ [*Gasparik et al.*, 1994] and

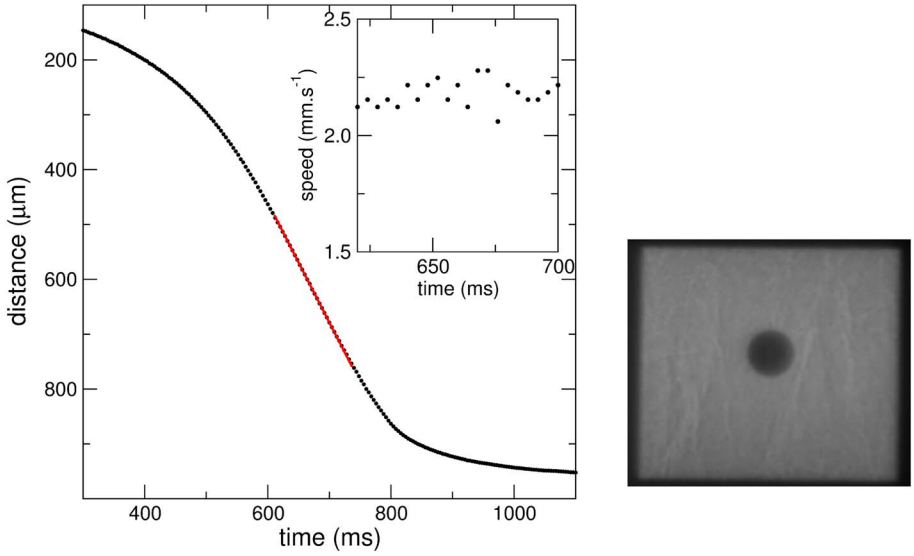

Figure 2. (left) Analysis of the sphere fall in natural $MgSiO_3$ melt at 3.1 GPa and 1950 K (N.B.: time "0" was chosen ahead of the sphere descent to fully capture it but was delayed by a minimum of 30 s from the time at which target power was reached). The red line is the linear regression fit at the equilibrium regime. (left, inset) Speed of the falling sphere in the equilibrium regime. Each point (left figure and inset) corresponds to one frame. (right) Radiographic frame taken during the corresponding fall. The black shadows are defined by the X-ray beam entrance slits horizontally (1 mm × 1mm) and by the WC anvils of the press horizontally.

Table 2. Experimental Run Conditions and Results

P (GPa)	*T* (K)	Viscosity (mPa s)
	$CaSiO_3$	
1.1(0.2)	1873(50)	184.2(2.6)
1.8(0.2)	1883(50)	167.8(1.7)
3.4(0.4)	1973(50)	159.5(6.7)
4.3(0.2)	1913(50)	116.6(1.4)
5.9(0.4)	2173(50)	110.3(2.1)
6.1(0.5)	2008(50)	100.8(1.4)
6.4(0.4)	2128(50)	103.6(1.6)
6.8(0.3)	2063(50)	103.5(1.8)
	$MgSiO_3$ #1	
1.1(0.2)	1823(50)	156.9(1.0)
2.6(0.2)	1923(50)	98.1(0.8)
3.1(0.2)	1948(50)	89.6(1.1)
4.5(0.2)	1923(50)	66.7(0.5)
5.2(0.5)	2023(50)	54.4(0.8)
6.1(0.3)	2153(50)	55.0(1.2)
6.3(0.2)	2148(50)	53.5(0.7)
7.0(0.4)	2123(50)	60.1(0.7)
7.6(0.5)	2203(50)	61.4(1.1)
	$MgSiO_3$ #2	
4.4(0.2)	1878(55)	61.7(1.7)
1.0(0.2)	2113(70)	95.8(5.1)
2.6(0.2)	2143(70)	68.9(3.5)
4.3(0.4)	2163(75)	52.6(2.0)
4.5(0.5)	2113(70)	43.0(1.8)
4.8(0.2)	2198(80)	60.1(0.4)
5.7(0.2)	2168(90)	44.3(1.3)
5.8(0.4)	2118(95)	45.3(0.9)
6.6(0.2)	2243(60)	40.2(0.6)

$MgSiO_3$ #1 [*Presnall and Gasparik*, 1990] and along the 2155 ± 43 K isotherm for $MgSiO_3$ #2 melt plus two additional points at 4.4 GPa and 1878 K and 6.6 GPa and 2243 K (Table 2). A high-speed frame rate camera (250 frames per second) captures the descent of the sphere as it passes through the liquid. A distance/time curve (Figure 2) is calculated from the descent of the sphere, from which the terminal velocity of the sphere can be extracted. Viscosity is then calculated using Stokes' law:

$$\eta = \frac{2gr_s^2(\rho_s - \rho_l)W}{9vE} \quad (1)$$

where r_s is the radius of the sphere, *s* and *l* are the densities of the sphere and the liquid, respectively, at a given pressure and temperature, and $g = 9.803$ m s^{-1} is the gravitational acceleration. *W* and *E* are correction factors that account for the wall and end-effects of a finite cylindrical container [*Faxèn*, 1922]. The radii r_s of the rhenium spheres, as determined from X-ray shadowgraph images using the high-resolution camera, ranged between 54 and 93 μm, where the largest uncertainty was 2 μm. The density of the spheres was calculated using the third-order Birch-Murnaghan equation of state, accounting for the thermal expansion of rhenium (6.2×10^{-6} K^{-1}) [*Vohra et al.*, 1987]. The density of melts at high *P* was taken from the equation of state of molten $MgSiO_3$ [*Petitgirard et al.*, 2015] (derived from glass density data), of $CaSiO_3$ glass [*Shimoda et al.*, 2005]

corrected for temperature effects [*Matsui*, 1996], and corrected for the effect of water [*Agee*, 2008]. No convection movements could be seen on the radiographic images, as expected from the very low Rayleigh number for our system. Indeed, using (2)

$$Ra = \frac{\alpha \rho g \Delta T h^3}{\kappa \mu} \quad (2)$$

and the following values for the parameters: 7×10^{-5} K^{-1} for α, the thermal expansion coefficient, 3000 kg m^{-3} for the density ρ, 9×81 m s^{-2} for g, a mean sample height of 1 mm, a maximum thermal gradient of 100 K using the estimate of 40 K/mm [*Rubie et al.*, 1993], thermal diffusivity κ of 7×10^{-5}, and viscosity μ of 100 mPa s (in the mean range of the present results), one finds Ra = 18.75, i.e., 2 orders of magnitude lower than the critical value for the start of convection.

4. Discussion

Viscosity decreases systematically with increased *P* (Figure 3), with a pronounced drop below 4–5 GPa and a flattening at higher *P*. Ambient *P* data [*Urbain et al.*, 1982] nicely complement our observed trends back to room *P* for all three compositions, indicating that the minor chemical deviations of our natural samples from pure end members compositions do not affect the viscosity noticeably. There is a marked *T* dependence at ambient *P*, with a factor two difference for $MgSiO_3$ viscosity over a 170 K *T* range between the lowest investigated *T* (i.e., 1987 K) and 2157 K [*Urbain et al.*, 1982], versus only 20% viscosity variation at 4.3 GPa over a 285 K range (Figure 3 and Table 2). This weakening of the *T* dependence upon increased *P* had also been reported for Fe_2SiO_4 melt, with a twofold drop of viscosity at ambient *P* over a 250 K range (1439 K–1685 K) that vanishes above 6 GPa, the 2123 K point from *Spice et al.* [2015] at 9.2 GPa lying within the error bars on the 1873 K isothermal trend. A slight but noticeable viscosity increase above 6.5 GPa is observed only for the $MgSiO_3$ #1 composition that contains 2.38 wt% Al_2O_3. This might be due to the increase of the Al-O coordination number that indeed takes place in this *P* range [*Drewitt et al.*, 2015]; we nonetheless note that only $MgSiO_3$ #1 was studied up to 7.6 GPa, while $MgSiO_3$ #2 and $CaSiO_3$ were only studied up to 6.8 GPa (Table 2).

Molten enstatite ($MgSiO_3$) has a lower viscosity than wollastonite ($CaSiO_3$) melt. The latter may be stiffer in relation with its structure. The short-range order is stronger in $CaSiO_3$ melt than in $MgSiO_3$ melt, as expressed by the first sharp diffraction peak (FSDP) that is much sharper on experimental form factors [*Funamori et al.*, 2004]. Besides, the FSDP intensity drops with *P* for $MgSiO_3$ melt. In contrast, Ca atoms are more weakly ordered than Mg, with a much wider distribution of the Ca–O bond than the Mg–O bond in both glasses and melts. Indeed, neutron diffraction data on a range of $(Mg_x,Ca_{1-x})SiO_3$ glasses [*Cormier and Cuello*, 2013] show that the Ca–O bond is both larger (2.2–2.3 Åversus 1.8 Å) and with a broader distribution than the Mg–O bond. Stronger Mg–O bonds might thus weaken the SiO_2 network, an effect not encountered for $CaSiO_3$ melts. A stronger SiO_2 network in $CaSiO_3$ melts would explain both their higher viscosity and glass-forming ability. This structural control on viscosity might also be expressed as a correlation between viscosity and cations atomic radii, whereby cation radii influence voids size. Viscosity of $CaSiO_3$ is the highest, consistent with ionic radius of Ca being the largest.

The effect of *P* on the viscosity of molten diopside was first investigated by ex situ measurements [*Scarfe et al.*, 1987; *Taniguchi*, 1992], whereby the distance fallen by spheres (SiC and BN) on samples recovered from high *P-T* conditions was used to estimate the settling velocity, a daunting task without precise in situ fall time measurements. First quantitative in situ X-ray radiographic measurements on diopside [*Reid et al.*, 2003] melts were interpreted as an initial increase of viscosity with *P* followed by a decrease. But if only the viscosity data for fully molten samples are considered, they agree well with the present data, with a marked viscosity decrease observed along the melting curve of diopside (Figure 3). *Liebske et al.* [2005] measured the viscosity of molten peridotite up to 13 GPa using a sphere trap on top of the sample to prevent the sphere from falling within the large *T* interval between solidus and liquidus, while another sphere was embedded within the peridotitic sample. The results were interpreted as an increase of viscosity up to 8 GPa, followed by a decrease, and were fitted with both Arrhenian and Vogel-Fulcher-Tamman equations modified empirically to account for the complex *P* behavior. However, spheres falling from a sphere trap show linear distance-time path while spheres located in peridotite powder show nonuniform velocity, indicating that the terminal velocity was not reached with the possibility that such data points overestimated viscosity as pointed out by *Liebske et al.* [2005]. If only spheres falling from within the trap are considered, a constant viscosity of ~20 mPa s is

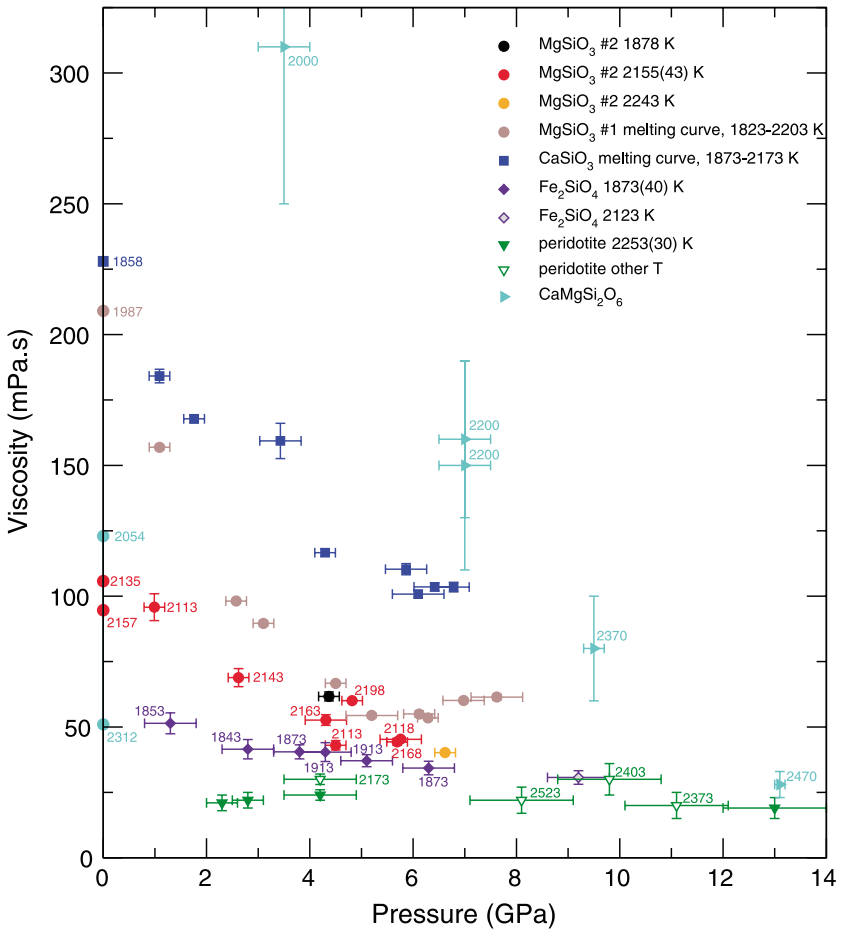

Figure 3. Viscosity of mafic melts as a function of pressure. $MgSiO_3$ and $CaSiO_3$ data from this work at high *P*, from *Urbain et al.* [1982] at ambient *P*, Fe_2SiO_4 data from *Spice et al.* [2015], peridotite from *Liebske et al.* [2005] (falls from sphere embedded in the density trap), and $CaMgSi_2O_6$ from *Reid et al.* [2003] excluding the two data points for which full melting could not be confirmed by the authors due to close proximity to the liquidus. Ambient *P* points are from *Urbain et al.* [1982]. For data sets collected along near isotherms, the value given in brackets is the magnitude of *T* variation.

observed throughout the *P* range at *T*=2223–2283 K. Molten silicates indeed may not have Arrhenian behavior but rather obey the Adam-Gibbs model [*Richet*, 1984] whereby the relaxation time is inversely proportional to the average probability of structural rearrangement which depends on the configurational entropy. This is consistent with the *T* dependence vanishing at high *P* as the probability of structural rearrangements is very low as the packing limit has been reached.

Considering that we have by now investigated three major end members of depolymerized melts, i.e., $MgSiO_3$, $CaSiO_3$, and Fe_2SiO_4[*Spice et al.*, 2015], any cotectic liquid in the system olivine-pyroxene is bound to also have a decreasing viscosity with increasing *P*. Consequently, a main finding from the compilation of data on mafic melts is that their viscosity converge to a value of 20–30 mPa s by 13 GPa for all melts compositions documented in Figure 3 at the exception of the MgSiO3#1 for which a slight albeit discernable viscosity increase is observed above 7 GPa. This common value of 20–30 mPa s, also reported for B_2O_3 a simple oxide melt [*Brazhkin et al.*, 2010], is lower than usual estimates for near-liquidus ultramafic melts of 100 mPa s [*Solomatov*, 2000]. Very interestingly, 13 GPa is the neutral buoyancy *P* for komatiite melts in the terrestrial mantle [*Robin-Popieul et al.*, 2012] and more generally for mantle melts 10–12 GPa [*Lee et al.*, 2010]. The lowest viscosity values at this *P* will counteract the reduced density contrast and favor melt extraction.

Structural rearrangements in magmas are numerous at ambient/low *P*, with voids induced by the melt polymerization. The latter collapse under *P*, a process nearly completed by 5 GPa as the tetrahedral packing limit is reached [*Wang et al.*, 2014]. The universal drop of viscosity reported here is attributed to the collapse of

voids and consequent reduction in size of the diffusing units and is, therefore, most pronounced in the most polymerized melts. Similarly, the decrease of viscosity upon compression for B_2O_3 melt was correlated with the disappearance of the medium-range order (boroxol rings), and the increase of B coordination number from 3 to 3.45, although the latter occurs only above 4.5 GPa once most of the viscosity decrease is completed [*Brazhkin et al.*, 2010]. The initial decrease of viscosity with *P* and its flattening at high *P* has been widely reported from experiments for a range of magmatic compositions, and there has been much discussion about the potential rise of viscosity as *P* is further increased. Besides theoretical predictions, the viscosity of molten basalt has been reported to increase above 5 GPa [*Sakamaki et al.*, 2013]. However, only one data point was clearly at a higher viscosity but had been collected at 5.33 GPa and 1990 K, i.e., quite close to the solidus (~1925 K–1975 K depending on basalt composition [*Tsuruta and Takahashi*, 1998; *Yasuda et al.*, 1994]). Theoretical studies predict an increase over 3 orders of magnitude for $MgSiO_3$ and $CaSiO_3$ melts on the 4000 K isotherm over the mantle *P* range [*Karki and Strixrude*, 2010; *Verma and Karki*, 2012], and the initial drop with *P* has been predicted only on the 3000 K isotherm but neither at lower or higher *T*. Once the packing limit of silicate melts has been reached [*Wang et al.*, 2014], there are no difference in atom-void structure among these fully depolymerized silicate melts, and as a result, viscosity of these melts converges into a constant value. There is no obvious reason why viscosity should go up again at higher *P* unless the interparticle interaction changes. This might occur in relation with Si coordination change above 15 GPa, while changes of CN of Ca, Mg, and Fe are finished around 10–15 GPa and that of Al is mostly completed (see *Sanloup* [2016], for a compilation). However, molten basalts laser heated using diamond-anvil cells systematically quench as fully crystalline assemblages from *P* above 10 GPa and up to 60 GPa, while they quench as glasses below 10 GPa [*Sanloup et al.*, 2013b]. Although not a quantitative argument, this indicates that the viscosity of the melt at 10 GPa and above is low enough for crystallization to occur during the quench to room *T*, while glass ability is favored at lower *P* where the viscosity is higher. Therefore, at least in the case of molten basalt, the viscosity does not seem to increase up to its low *P* values. This discussion highlights the crucial need to develop viscosity measurements on melts at higher *P* than currently available.

5. Conclusions

The viscosity of two pyroxene melt compositions studied here ($MgSiO_3$ and $CaSiO_3$) decreases with *P*, initially at a very fast rate, and then at a slower rate. The comparison with previous results obtained on molten Fe_2SiO_4 [*Spice et al.*, 2015], $CaMgSi_2O_6$ [*Reid et al.*, 2003], and molten peridotite [*Liebske et al.*, 2005] shows a convergence of their viscosity values ~13 GPa toward 20–30 mPa s, while the *T* effect vanishes above 5 GPa. Further viscosity increase at higher *P*, predicted by theoretical calculations, remains to be observed, and higher *P* experimental setups are needed to confirm it. A main geophysical consequence is that the deeper the mantle melts, the less viscous and more pervasive they will be, even in the absence of carbonates. This effect coincides with the neutral buoyancy postulated for kimberlitic melts at 13 GPa [*Robin-Popieul et al.*, 2012] and ultramafic melts at 10–12 GPa [*Lee et al.*, 2010]. Magma oceans therefore have lower viscosities than previously accounted for, and small planets or superficial magma oceans are likely to be much less viscid than deep magma oceans.

Acknowledgments
The research leading to these results has received funding from the European Community's Seventh Framework Programme (FP7/2007-2013) under grant agreements 312284 and 259649 (European Research Council starting grant to C.S.). High-pressure experiments were performed at HPCAT (Sector 16), Advanced Photon Source (APS), Argonne National Laboratory. HPCAT operations are supported by DOE-NNSA under award DE-NA0001974 and DOE-BES under award DE-FG02-99ER45775, with partial instrumentation funding by NSF. APS is supported by DOEBES, under contract DE-AC02-06CH11357. C.L. is funded by French state funds managed by the ANR within the Investissements d'Avenir programme under reference ANR-11-IDEX-0004-02 (cluster of Excellence MATISSE led by Sorbonne Universités). We thank the Laboratoire d'Etude des Elements Légers, NIMBE, CEA Saclay for their assistance during ERDA analysis. We acknowledge Y. Wang for discussion, O. Boudouma for assistance with the SEM imaging, M. Fialin for assistance with the electron microprobe analyses, and C. Kenney-Benson for providing cell-assembly parts. X-ray radiographic data associated with this research are located at http://hestia.istep.upmc.fr:8080/sharing/Rm1JbqgMG.

References

Agee, C. B. (2008), Static compression of hydrous silicate melt and the effect of water on planetary differentiation, *Earth Planet. Sci. Lett.*, *265*, 641–654.

Brazhkin, V. V., I. Farnan, K.-I. Funakoshi, M. Kanzaki, Y. Katayama, A. G. Lyapin, and H. Saitoh (2010), Structural transformations and anomalous viscosity in the B2O3 melt under high pressure, *Phys. Rev. Lett.*, *105*(11), 115701, doi:10.1103/PhysRevLett.105.115701.

Bureau, H., C. Raepsaet, H. Khodja, A. Carraro, C. Aubaud, and S. Kubsky (2009), Determination of hydrogen content in geological samples using elastic recoil detection analysis (ERDA), *Geochim. Cosmochim. Acta*, *73*, 3311–3322.

Carlson, R. W., E. Garnero, T. M. Harrison, J. Li, M. Manga, W. F. McDonough, S. Mukhopadhyay, B. Romanowicz, D. Rubie, Q. Williams, and S. Zhong (2014), How did early earth become our modern world?, *Annu. Rev. Earth Planet. Sci.*, *42*, 151–178.

Cormier, L., and G. J. Cuello (2013), Structural investigation of glasses along the $MgSiO_3$-$CaSiO_3$ join: Diffraction studies, *Geochim. Cosmochim. Acta*, *122*, 498–510, doi:10.1016/j.gca.2013.04.026.

Drewitt, J. W. E., S. Jahn, C. Sanloup, C. de Grouchy, G. Garbarino, and L. Hennet (2015), Development of chemical and topological structure in aluminosilicate liquids and glasses at high pressure, *J. Phys.*, *27*(105), 103.

Elkins-Tanton, L. T. (2012), Magma oceans in the inner solar system, *Annu. Rev. Earth Planet. Sci.*, *40*, 113–139, doi:10.1146/annurev-earth-042711-105503.

Faxèn, H. (1922), The resistance against the movement of a rigour sphere in viscous fluids, which is embedded between two parallel layered barriers, *Ann. Phys.*, *68*, 89–119.

Funamori, N., S. Yamamoto, T. Yagi, and T. Kikegawa (2004), Exploratory studies of silicate melt structure at high pressures and temperatures by in situ X-ray diffraction, *J. Geophys. Res.*, *109*, B03203, doi:10.1029/2003JB002650.

Gasparik, T., K. Wolf, and C. Smith (1994), Experimental determination of phase relation in the $CaSiO_3$ system from 8 to 15 GPa, *Am. Mineral*, *79*(11–12), 1219–1222.

Hoink, T., J. Schmalzl, and U. Hansen (2006), Dynamics of metal-silicate separation in a terrestrial magma ocean, *Geochem. Geophys.*, *7*, Q09008, doi:10.1029/2006GC001268.

Karki, B. B., and L. Strixrude (2010), Viscosity of $MgSiO_3$ at Earth's mantle conditions: Implications for an early magma ocean, *Science*, *328*, 740–742, doi:10.1126/science.1188327.

Kono, Y., T. Irifune, Y. Higo, T. Inoue, and A. Barnhoorn (2010), P-V-T relation of MgO derived by simultaneous elastic wave velocity and in situ X-ray measurements: A new pressure scale for the mantle transition region, *Phys. Earth Planet. Int.*, *183*, 196–211.

Kono, Y., C. Kenney-Benson, C. Park, G. Shen, and Y. Wang (2013), Anomaly in the viscosity of liquid KCl at high pressures, *Phys. Rev. B*, *87*, 24302.

Kono, Y., C. Park, C. Kenney-Benson, G. Shen, and Y. Wang (2014), Toward comprehensive studies of liquids at high pressures and high temperatures: Combined structure, elastic wave velocity, and viscosity measurements in the Paris-Edinburgh cell, *Phys. Earth Planet. Int.*, *228*, 269–280, doi:10.1016/j.pepi.2013.09.006.

Kono, Y., C. Kenney-Benson, Y. Shibazaki, C. Park, G. Shen, and Y. Wang (2015), High-pressure viscosity of liquid Fe and FeS revisited by falling sphere viscometry using ultrafast X-ray imaging, *Phys. Earth Planet. Int.*, *241*, 57–64, doi:10.1016/j.pepi.2015.02.006.

Lee, C.-T. A., P. Luffi, T. Höink, J. Li, R. Dasgupta, and J. Hernlund (2010), Upside-down differentiation and generation of a primordial lower mantle, *Nature*, *463*, 930–935.

Liebske, C., B. Schmickler, H. Terasaki, B. Poe, A. Suzuki, K. Funakoshi, R. Ando, and D. Rubie (2005), Viscosity of peridotite liquid up to 13 GPa: Implications for magma ocean viscosities, *Earth Planet. Sci. Lett.*, *240*, 589–604, doi:10.1016/j.epsl.2005.10.004.

Maas, C., and U. Hansen (2015), Effects of Earth's rotation on the early differentiation of a terrestrial magma ocean, *J. Geophys. Res. Solid Earth*, *120*, 7508–7525, doi:10.1002/2015JB012053.

Matsui, M. (1996), Molecular dynamics simulation of structures, bulk moduli, and volume thermal expansivities of silicate liquids in the system CaO-MgO-Al_2O_3-SiO_2, *Geophys. Res. Lett.*, *23*(4), 395–398, doi:10.1029/96GL00260.

Moeller, A., and U. Hansen (2013), Influence of rotation on the metal rain in a Hadean magma ocean, *Geochem. Geophys.*, *14*(4), 1226–1244, doi:10.1002/ggge.20087.

Nisbet, E. G. (1982), *The Tectonic Setting and Petrogenesis of Komatiites*, Allen and Unwin, pp. 501–520, Concord, Mass.

Petitgirard, S., W. J. Malfait, R. Sinmyo, I. Kupenko, L. Hennet, D. Harries, T. Dane, M. Burghammer, and D. C. Rubie (2015), Fate of $MgSiO_3$ melts at core-mantle boundary conditions, *Proc. Natl. Acad. Sci. U.S.A.*, *112*(46), 14,186–14,190, doi:10.1073/pnas.1512386112.

Presnall, D., and T. Gasparik (1990), Melting of enstatite ($MgSiO_3$) from 10 to 16.5 GPa and the forsterite (Mg_2SiO_4) – Majorite ($MgSiO_3$) eutectic at 16.5 GPa – Implications for the origin of the mantle, *J. Geophys. Res.*, *95*(B10), 15,771–15,777, doi:10.1029/JB095iB10p15771.

Reid, J., A. Suzuki, K. Funakoshi, H. Terasaki, B. Poe, D. Rubie, and E. Ohtani (2003), The viscosity of $CaMgSi_2O_6$ liquid at pressures up to 13 GPa, *Phys. Earth Planet. Int.*, *139*, 45–54, doi:10.1016/S0031-9201(03)00143-2.

Richet, P. (1984), Viscosity and configurational entropy of silicate melts, *Geochim. Cosmochim. Acta*, *48*, 471–483.

Robin-Popieul, C. M., N. T. Arndt, C. Chauvel, G. R. Byerly, A. V. Sobolev, and A. Wilson (2012), A new model for Barberton Komatiites: Deep critical melting with high melt retention, *J. Petrol.*, *53*(11), 2191–2229, doi:10.1093/petrology/egs042.

Rubie, D., S. Karato, H. Yan, and H. O'Neill (1993), Low differential stress and controlled chemical environment in multianvil high-pressure experiments, *Phys. Chem. Miner.*, *20*(5), 315–322.

Sakamaki, T., Y. Wang, C. Park, T. Yu, and G. Shen (2012), Structure of jadeite melt at high pressures up to 4.9 GPa, *J. Appl. Phys.*, *111*, 112623.

Sakamaki, T., A. Suzuki, H. Terasaki, S. Urakawa, Y. Katayama, K. Funakoshi, J. Hernlund, and M. Ballmer (2013), Ponded melt at the boundary between the lithosphere and asthenosphere, *Nat. Geosci.*, *6*, 1041–1044, doi:10.1063/1.4726246.

Sanloup, C. (2016), Density of magmas at depth, *Chem. Geol.*, *429*, 51–59, doi:10.1016/j.chemgeo.2016.03.002.

Sanloup, C., J. W. E. Drewitt, C. Crépisson, Y. Kono, C. Park, C. McCammon, L. Hennet, S. Brassamin, and A. Bytchkov (2013a), Structure and density of molten fayalite at high pressure, *Geochim. Cosmochim. Acta*, *118*, 118–128.

Sanloup, C., J. W. E. Drewitt, Z. Konôpková, P. Dalladay-Simpson, D. M. Morton, N. Rai, W. van Westrenen, and W. Morgenroth (2013b), Structural change in molten basalt at deep mantle conditions, *Nature*, *503*, 104–107.

Scarfe, C. M., B. O. Mysen, and D. Virgo (1987), Pressure dependence of the viscosity of silicate melts, in *Magmatic Processes: Physicochemical Principles*, edited by B. O. Mysen, pp. 59–67, Geochem. Soc., Pa.

Shimoda, K., H. Miyamoto, A. Kikuchi, K. Kusaba, and M. Okuno (2005), Structural evolutions of $CaSiO_3$ and $CaMgSi_2O_6$ metasilicate glasses by static compression, *Chem. Geol.*, *222*(1–2), 83–93, doi:10.1016/j.chemgeo.2005.07.003.

Sobolev, A. V., E. V. Asafov, A. A. Gurenko, N. T. Arndt, V. G. Batanova, M. V. Portnyagin, D. Garbe-Schoenberg, and S. P. Krasheninnikov (2016), Komatiites reveal a hydrous Archaean deep-mantle reservoir, *Nature*, *531*(7596), 628–632, doi:10.1038/nature17152.

Solomatov, V. S. (2000), *Fluid dynamics of a terrestrial magma ocean*, Univ. Ariz. Press, pp. 323–328, Tucson, Ariz., doi:10.1029/92JE02839.

Solomatov, V. S. (2007), *Magma Oceans and Primordial Mantle Differentiation*, Elsevier, pp. 91–119, Amsterdam.

Spice, H., C. Sanloup, B. Cochain, C. de Grouchy, and Y. Kono (2015), Viscosity of liquid fayalite up to 9 GPa, *Geochim. Cosmochim. Acta*, *148*, 219–227.

Stolper, E., D. Walker, B. H. Hager, and J. F. Hays (1981), Melt segregation from partially molten source regions: The importance of melt density and source region size, *J. Geophys. Res.*, *86*, 6261–6271.

Taniguchi, H. (1992), Entropy dependence of viscosity and the glass-transition temperature of melts in the system diopside-anorthite, *Contrib. Mineral. Petrol.*, *109*, 295–303.

Tsuruta, K., and E. Takahashi (1998), Melting study of an alkali basalt JB-1 up to 12.5 GPa: Behavior of potassium in the deep mantle, *Phys. Earth Planet. Int.*, *107*, 119–130.

Urbain, G., Y. Bottinga, and P. Richet (1982), Viscosity of liquid silica, silicates and alumino-silicates, *Geochim. Cosmochim. Acta*, *46*, 1061–1072.

Verma, A. K., and B. B. Karki (2012), First-principles study of self-diffusion and viscous flow in diopside ($CaMgSi_2O_6$) liquid, *Am. Mineral.*, *97*(11–12), 2049–2055, doi:10.2138/am.2012.4123.

Vohra, Y., S. Duclos, and A. Ruo (1987), High-pressure X-ray diffraction studies on rhenium up to 216 GPa (2.16 Mbar), *Phys. Rev. B*, *36*, 9790–9792, doi:10.1103/PhysRevB.36.9790.

Wang, Y. B., T. Sakamaki, L. B. Skinner, Z. Jing, T. Yu, Y. Kono, C. Park, G. Shen, M. L. Rivers, and S. R. Sutton (2014), Atomistic insight into viscosity and density of silicate melts under pressure, *Nat. Commun.*, *5*, 3241, doi:10.1038/ncomms4241.

Whittington, A., P. Richet, and F. Holtz (2000), Water and the viscosity of depolymerized aluminosilicate melts, *Geochim. Cosmochim. Acta*, *64*, 3725–3736.

Yasuda, A., T. Fuji, and K. Kurita (1994), Melting phase relations of an anhydrous mid-ocean ridge basalt from 3 to 20 GPa: Implications for the behavior of subducted oceanic crust in the mantle, *J. Geophys. Res.*, *99*, 9401–9414.

Zhang, J., and C. Herzberg (1994), Melting experiments on anhydrous peridotite KLB-1 from 5.0 to 22.5 GPa, *J. Geophys. Res.*, *99*(B9), 17,729–17,742, doi:10.1029/94JB01406.